

# Emission of biased green quantum wells in time and wavelength domain

Ulrich T. Schwarz

Department of Physics, Regensburg University  
93040 Regensburg, Germany

## ABSTRACT

Carrier lifetime and efficiency droop of green light emitting InGaN QWs in LEDs and laser diodes (LD) are discussed in term of Shockley–Read–Hall, radiative, and Auger–like recombination. The carrier lifetime, spectral shift, and carrier density as function of current density was measured by time–resolved electroluminescence with a streak camera. The current density was varied from very low for the LEDs to threshold for the LD. The transition from spontaneous emission in the low carrier density regime to stimulated emission in the high carrier regime is continuous. A comparison with Hakki–Paoli optical gain spectra provides evidence for a significant contribution of stimulated emission already at intermediate current densities. Stimulated emission is discussed as possible contribution to efficiency droop. A wavelength dependency of the lifetime is certainly caused by stimulated emission. Slope efficiency of the laser diode provides a lower limit for the injection efficiency of the LD. Time–resolved electroluminescence spectroscopy with applied bias demonstrates the variation of radiative recombination and consequently carrier lifetime with applied bias. Under certain conditions for modulated operation more light is emitted during times of zero bias than during forward bias.

**Keywords:** InGaN LED, efficiency, droop, rate equations, built–in potential, Auger losses

## 1. INTRODUCTION

All important applications of solid state lighting and LED projection based on LEDs need high optical power and power density.<sup>1,2</sup> High power LEDs are typically specified for a current of the order of 1 A through an area of 1 mm<sup>2</sup>. A hotly debated question is the drop of efficiency in the range of high driving currents. The efficiency as function of current first rises, as radiative recombination dominates over nonradiative recombination, than drops again. This effect is called ‘efficiency droop’ and can be described by a nonradiative process proportional to the cube of the carrier density.<sup>3</sup> The Auger scattering process has this dependency, yet for wide bandgap semiconductors Auger scattering should be a small effect. Hader *et al.* rule out the standard Auger process as mechanisms responsible for the droop, while still arguing for an Auger–like (i.e.  $\propto N^3$ ) loss term.<sup>4</sup> Another possible mechanism is a drop in carrier injection efficiency  $\eta_{inj}$ .<sup>5–7</sup> Schubert *et al.* show convincingly that this explanation leads to the prediction of a reduction of the droop with reduced piezoelectric fields in the active region. This was experimentally verified for LEDs with quaternary barriers<sup>5</sup> and InGaN/InGaN quantum wells (QW) and barriers.<sup>8</sup> Thermal overrolling as loss mechanism was ruled out, both by LEDs with optimized heat sinking schemes, by pulsed measurements with low duty cycles, and by the comparison of resonantly excited photoluminescence and electroluminescence.<sup>5</sup>

One commonly used argument against the Auger–like mechanism are laser diodes (LD), as they work in the high current density regime. A strong Auger effect, so the line of the argument, would inhibit lasing. A different argument connects slope efficiency of LDs with droop. The fact that a low  $\eta_{inj}$  is in contradiction to the high slope efficiency achieved for violet and blue LDs<sup>9,10</sup> speaks against a drop in  $\eta_{inj}$  as origin of the droop.

In this article we measure decay times for LEDs and a LD for current densities ranging from low LED current densities to LD threshold current density. All three examined devices are comparable in their emission wavelength. We compared two LEDs emitting at 520 nm and 530 nm, respectively, with a blue LD with a lasing

---

Further author information:

Ulrich T. Schwarz: E-mail: ulrich.schwarz@physik.uni-regensburg.de, Telephone: +49 (0) 941 943 4213

wavelength of 470 nm which emits as LED in the low current regime at 510 nm. We measure and discuss the carrier density dependent carrier lifetime. One important argument is that stimulated emission determines the carrier lifetime also considerably below threshold, in the current regime of a high power LED.

We see no evidence for a drop in injection efficiency. The slope efficiency suggests a injection efficiency close to one above threshold. Yet we discuss that this does not immediately rule out  $\eta_{inj}$  as origin of droop in a LED.

We also discuss the impact of bias voltage on the radiative recombination time. The internal field in an InGaN quantum well in a LED or laser diode is given by the superposition of the piezoelectric field and the field due to the built-in potential of the pn junction. Therefore one can tweak the transition matrix element and emission wavelength by an applied bias voltage, e.g. for bias-dependent photoluminescence spectroscopy. For fast switching or modulation at frequencies of the order of the inverse carrier life time, carrier injection and emission can be separated temporally. One signature of this effect is a bright emission during zero or reverse bias after the driving pulse when the radiative recombination rate is at its maximum.<sup>11</sup> Modulation of the LED driving current might be a possible path to increase efficiency and color rendering index (CRI).

Overall we show that there is a smooth transition from a green LED via a blue LD operating as green LED, to a blue LD. On the one hand this smooth transition demonstrates that an Auger-like term is not in conflict with LD operation. On the other hand stimulated emission is important also below threshold and affects carrier recombination. In particular it causes a wavelength dependent carrier lifetime. While stimulated emission is the essential effect in LDs, it may also critically affect LED operation in the high current regime. We stress that both stimulated emission and bias voltage have to be considered in the interpretation of carrier lifetime measurements in InGaN quantum wells.

## 2. CARRIER DENSITY AND CARRIER LIFE TIME IN THE SIMPLE RATE EQUATION MODEL

To describe the carrier density in the regime of spontaneous emission we use the following time dependent rate equation for the carrier density:

$$\frac{dN}{dt} = -AN - BN^2 - CN^3 + \frac{\eta_{inj} J}{q_e} \quad (1)$$

This differential equation can be used to describe time-dependent experiments, e.g. photoluminescence or electroluminescence decay measurements, as well as stationary properties. The recombination terms on the right side are Shockley-Read-Hall (nonradiative) recombination, radiative recombination, and Auger scattering. The last term represents the current injection with injection efficiency  $\eta_{inj}$ . Current and two-dimensional carrier density are defined with respect to the LED or LD area  $A_{\square}$ .  $q_e$  is the elementary charge. In the rate equation carrier overflow and Auger scattering are both included as loss mechanisms. Yet throughout the article we assume that carrier overflow is negligible and set  $\eta_{inj} = 1$ . We will later justify this assumption when we discuss the slope efficiency of the LD. Regarding the  $N^3$  term, it was argued that Auger losses are negligible for wide band semiconductors. Hader *et al.* implemented the Auger process in a microscopic model for GaN-based quantum wells and ruled out the standard Auger process as origin of the droop.<sup>4</sup> Yet there is solid experimental evidence for a loss term of third order in carrier density, which is included as Auger or Auger-like term  $CN^3$  in Eq. 1.

The rate equation in the form of Eq. 1 is valid as long as stimulated emission can be neglected. For carrier densities close to lasing threshold, optical gain and a second rate equation for the photon density has to be included already in the simplest model. These two coupled differential equations are then capable to describe delay of lasing onset and relaxation oscillations. There are also limitations to this simple rate equation in the high carrier density and ultrafast regime. It was debated whether the dependency  $AN + BN^2 + CN^3$  applies at all for LDs. We refrain from that discussion and assume that Eq. 1 applies for not too fast modulation ( $< \text{GHz}$ ) and carrier densities below  $10^{12} \text{ cm}^{-2}$ .

The different recombination mechanisms result in a carrier density dependent carrier life time  $\tau(N)$ :

$$\tau^{-1} = A + BN + CN^2 = \tau_{nr}^{-1} + \tau_{rad}^{-1} + \tau_{Auger}^{-1}. \quad (2)$$

At low carrier densities, recombination is dominated by the nonradiative recombination, or  $\tau^{-1} = A$ . With increasing  $N$ , first the radiative recombination and then the Auger-like term become the dominant pathway.

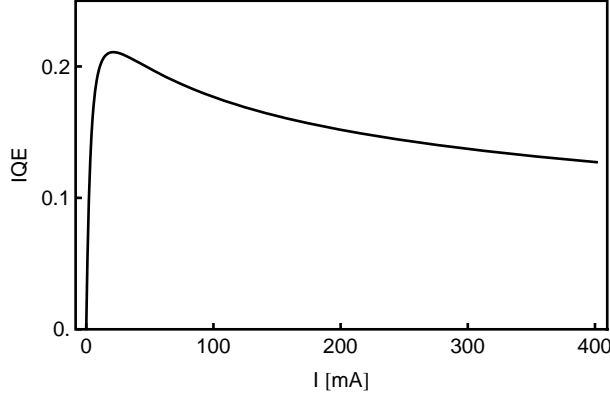


**Figure 1.** Internal quantum efficiency  $\eta_{IQE}$  as given by Eq. 5, calculated in the simple rate equation model Eq. 1. The parameters used are those given in Table 1 for the green LED1. The current was calculated for an area  $A_{\square} = (200 \mu\text{m})^2$ .

In the stationary case ( $dN/dt = 0$ ) the relation between current density  $J$  and carrier density is given as

$$\eta_{inj}J = \frac{q_e N}{\tau} \quad (3)$$

The carrier life time  $\tau(N)$  depends on carrier density, as given by Eq. 2. Current and current density are simply related as  $J = I/A_{\square}$ .

The spontaneous emission per area can be expressed by the radiative current density

$$J_{rad} = q_e B N^2. \quad (4)$$

The internal quantum efficiency  $\eta_{IQE}$  is the ratio of radiative current density to the current density injected into the quantum wells,

$$\eta_{IQE} = \frac{q_e B N^2}{q_e N / \tau} = B N \tau = \frac{\tau_{rad}^{-1}}{\tau_{nr}^{-1} + \tau_{rad}^{-1} + \tau_{Auger}^{-1}}. \quad (5)$$

In Fig. 1 the internal quantum efficiency is plotted as function of current for a LED with an area of  $A_{\square} = (200 \mu\text{m})^2$ . The maximum of the efficiency  $\eta_{IQE} \approx 0.2$  is reasonable for a green light emitter. The  $\eta_{IQE}$  curve shows the characteristic efficiency droop for higher current densities. This drop of the efficiency is caused by the Auger-like term. The  $A$ ,  $B$ , and  $C$  parameters used here and throughout the article are collected in table 1. The IQE curve of Fig. 1 was calculated with the parameters of the green LED1.

To measure carrier lifetime we use a streak camera (Hamamatsu M5680 with slow single sweep unit M5677) in combination with a fast electronic pulse generator (Hewlett Packard 8131A). The pulse length is variable in the range from 10 ns to several milliseconds. A resistance network with a  $10 \Omega$  shunt was used to measure current and voltage. The pulse rise and fall time was of the order of 10 ps. The time resolution is limited by trigger jitter. The fastest measured fall time of  $\approx 100$  ps provides an upper limit for the achieved temporal resolution. Measurements with the same setup are also described in Ref. [11].

**Table 1.** Samples and simulation parameters used for this work.

sample	$A$ [ $\text{ns}^{-1}$ ]	$B$ [ $\text{cm}^2 \text{ns}^{-1}$ ]	$C$ [ $\text{cm}^4 \text{ns}^{-1}$ ]	LED peak wavelength	lasing wavelength
LD470	$7 \times 10^{-3}$	$2 \times 10^{-7}$	$2 \times 10^{-20}$	510 nm	470 nm
LED1	$7 \times 10^{-3}$	$2 \times 10^{-6}$	$1 \times 10^{-18}$	520 nm	—
LED2	$7 \times 10^{-3}$	$1 \times 10^{-5}$	$3 \times 10^{-17}$	530 nm	—

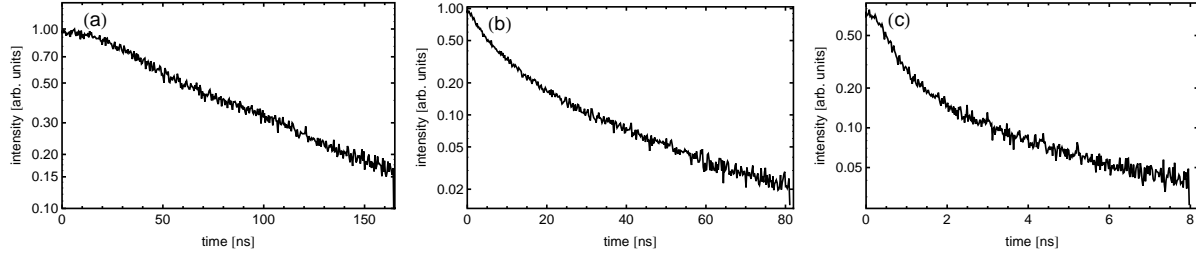


**Figure 2.** Decay of electroluminescence intensity measured for LD470 after the falling edge of a 400 ns long electrical driving pulse. The current was (a)  $I = 0.16$  mA, (b)  $I = 9.4$  mA, and (c)  $I = 41$  mA.

The decay of the electroluminescence signal at the end of a 400 ns pulse is shown in Fig. 2 for the 470 nm LD for three different currents  $I = 0.16$  mA,  $I = 9.4$  mA, and  $I = 41$  mA. These time traces show the characteristic decay mechanisms discussed throughout the article. The pulse length of 400 ns was chosen in order to achieve a stationary equilibrium for the carrier density during the pulse while preventing heating. For the lowest current density the decay is single exponential (see Fig. 2a). For intermediate current densities, the decay deviates from the single exponential behavior (see Fig. 2b). This is a consequence of the carrier density dependent decay time  $\tau(N)$  as given by Eq. 2. For even higher current densities, the curve shows a fast initial decay (see Fig. 2c). In this current regime close to lasing threshold ( $I_{th} \approx 43$  mA) optical gain becomes relevant, and stimulated emission causes the initial fast decay.

From measurements like those shown in Fig. 2 we extract the decay time. Decay rate (inverse decay time) and carrier density as function of current are plotted in Fig. 3. The decay rate plotted in Fig. 3b is the initial decay time, measured immediately after the falling edge of the driving pulse. Therefore it is the decay time corresponding to the equilibrium carrier density at the current density during the pulse. This allows to calculate the stationary carrier density during the pulse from Eq. 3. These are the values plotted in Fig. 3a. We will later show that the decay time is a function of the bias value. We neglect this effect for this first estimation of decay rates and carrier densities.

The measured decay rates for the green LEDs and the 470 nm LD approach the Shockley–Read–Hall recombination rate in the low current density regime. For higher carrier densities the recombination rate increases by one to three orders of magnitude. This behavior is universal for optimized standard LEDs or LDs emitting in the green spectral region. With standard we mean such which are based on thin InGaN quantum wells of *c*-plane orientation. For nonpolar or semipolar quantum wells the decay time is much shorter.

The black curves in Fig. 3 represent carrier density  $N$  and carrier life time  $\tau$  calculated with Eqs. 3 and 2 for the  $A$ ,  $B$ , and  $C$  parameters as given in table 1. The decay rates corresponding to the different recombination mechanisms are also indicated in this graph. The agreement of measurement and calculation is good up to a current of  $700$  A/cm<sup>2</sup>, or roughly  $J_{th}/4$ . For higher current densities, the decay rates grow faster than the  $C N^2$  term. The cause for this fast decay is stimulated emission, as will be shown in section 3. Because optical gain is not included in our rate equation, the carrier density calculated from the measured decay rate and current density decreases with increasing current in this regime (see Fig. 3a). The real carrier densities continues to increase along the black solid curve until threshold, where it is clamped. From Fig. 3a) the threshold carrier density can be estimated as  $N_{th} \approx 4 \times 10^{13}$  cm<sup>-2</sup>. This has to be compared with threshold carrier densities of  $N_{th} \approx 1.2 \times 10^{13}$  cm<sup>-2</sup> calculated for this 470 nm with a microscopic approach<sup>12</sup> and  $N_{th} \approx 0.9 \times 10^{13}$  cm<sup>-2</sup> calculated in a microscopic model for a 405 nm LD.<sup>13, 14</sup> The threshold carrier density calculated in a free electron, constant Fermi level model for this 470 nm LD was a factor 10 lower.<sup>15</sup>

The simple rate equation is also capable to simulate the temporal evolution of the electroluminescence during pulsed excitation, as demonstrated in the following comparison for LED1. With the rate equation Eq. 1 and the parameter set for LED1 in table 1 we simulated the electroluminescence of a green LED during and after a 200 ns

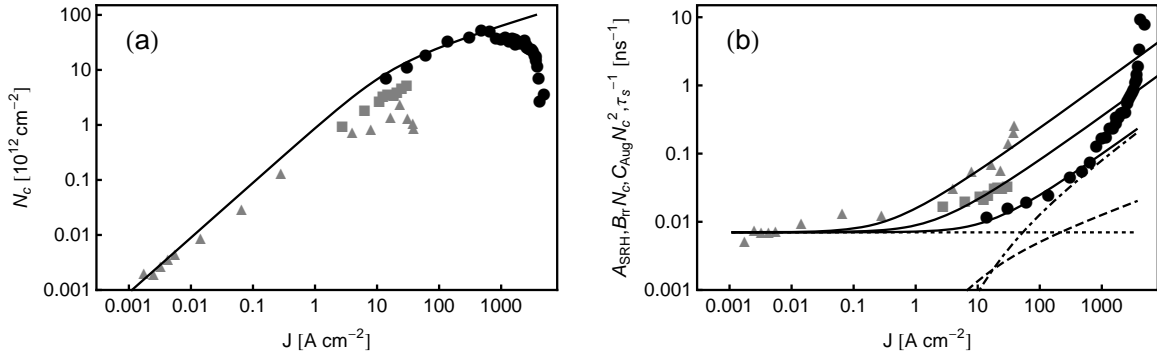


**Figure 3.** (a) carrier density and (b) decay rate for green light emitting quantum wells. The gray triangles and squares are measurements for LD1 and LD2, respectively. The black circles are measurements for a 470 nm LD. The solid curves in (b) are the total decay rate, Eq. 2, calculated with the respective parameters from table 1. For the LD470 the decay rates corresponding to Shockley–Read–Hall nonradiative recombination, radiative recombination, and Auger scattering are shown as dotted, dashed, and dot–dashed curves, respectively. The carrier density in (a) are calculated from the measured decay time and current density via Eq. 3.

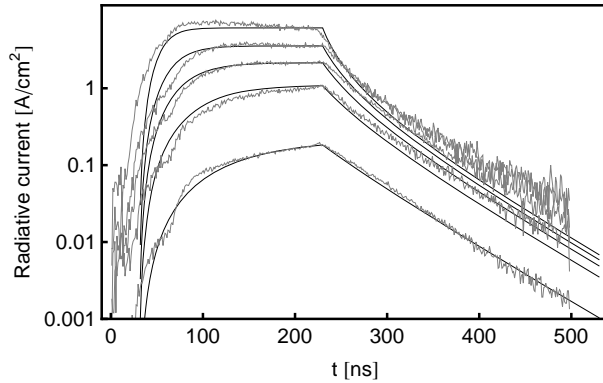


**Figure 4.** Time dependent luminescence for the green light emitting LED1. The electroluminescence was measured during and after a 200 ns electrical driving pulse. The applied currents are  $I = [0.55, 1.8, 3.3, 5.5, 10]$  mA.

long pulse and for different current densities. The simulated times traces and the corresponding experiment are shown in Fig. 4. The free parameter is a scaling factor for the light collecting efficiency of our experiment, i.e. the streak camera. Also, for the lowest curve the current was only estimated. The driving pulse is not an ideal rectangular pulse. Due to impedance mismatch and pulse generator peculiarities the leading edge shows a structure which is responsible for most of the deviation between simulation and experiment. Overall, the simulations agrees in the essential details with the experiment, both in the onset and decay of the electroluminescence signal. For low currents the decay is single exponential, while for high currents the decay rate depends on the carrier density.

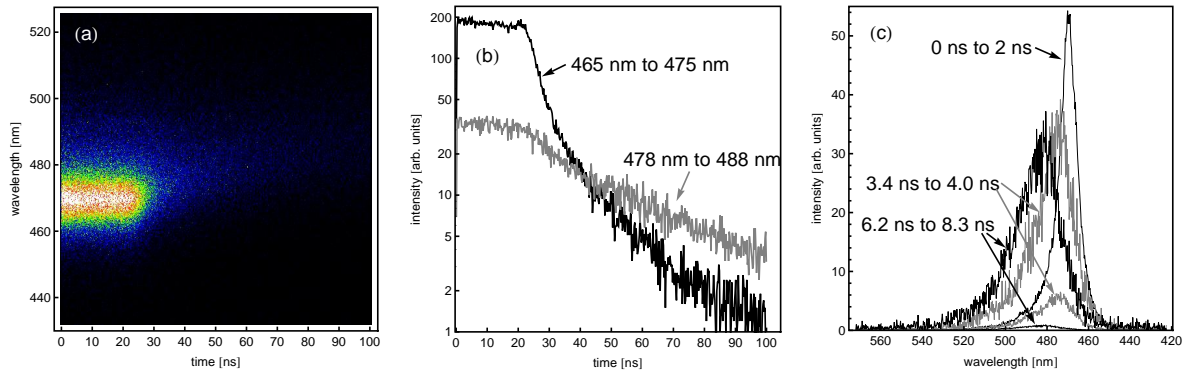


**Figure 5.** [Color online] Temporally and spectrally resolved decay of the electroluminescence at the trailing edge of a 400 ns long electrical driving pulse with current  $I = 41$  mA. (a) streak camera image, measured in photon counting mode; (b) time traces, spectrally integrated from 465 nm to 475 nm and from 478 nm to 488 nm; (c) spectra taken during the pulse, shortly after the pulse, and close to the end of the time window. The last two spectra are plotted in the original scale as well as scaled by factors of 6 and 40, respectively.

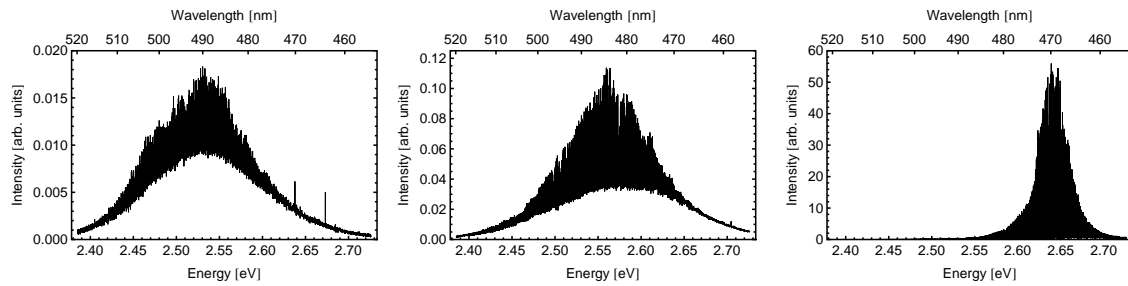


**Figure 6.** Electroluminescence spectra for a 470 nm LD taken with high spectral resolution spectrometer. The broad black areas consist of thousands of longitudinal Fabry–Perot modes of the laser cavity. The mode spacing is of the order of 0.05 nm, the individual modes are well resolved in this experiment. The spectra consist of approximately 40.000 points, 4.000 of which are plotted. The three spectra were measured at currents of  $I = 2$  mA,  $I = 5$  mA, and  $I = 40$  mA (from left to right). These spectra are used to calculate optical gain spectra with the Hakki–Paoli method.<sup>16, 17</sup>

### 3. CONTRIBUTION OF STIMULATED EMISSION TO CARRIER DECAY

In this section the impact of stimulated emission on the carrier decay rate will be shown. The measurements for the 470 nm LD nicely show the transition from spontaneous emission with carrier density dependent life time to stimulated emission. With the same LD we also measured the optical gain below threshold, employing the Hakki–Paoli method.<sup>15, 17</sup> The latter method derives the optical gain from the Fabry–Perot resonances of the amplified spontaneous emission spectra below threshold. Therefore the relation between the envelope of the spontaneous spectra and optical gain is well known.<sup>18</sup>

Figure 5a shows the streak camera measurement for the 470 nm LD at the trailing edge of a 400 ns pulse and with a current of  $I = 41$  mA, slightly below threshold. Axes are time and wavelength. The image was taken in photon counting mode. From  $t = 0$  ns to  $t \approx 2.5$  ns the driving pulse is still on. The spectral resolution of the spectrometer connected with the streak camera is not good enough to resolve the longitudinal Fabry–

Perot modes of the LD. So the spectrum is the envelope of many longitudinal modes centered around the lasing wavelength of 470 nm. The decay after the trailing edge of the pulse ( $t > 50$  ns) is clearly asymmetric, with shorter wavelength decaying faster than longer wavelength. Figure 5b shows the time trace of two spectral regions from the streak camera image. On the long wavelength side of the spectrum (478 to 488 nm) the intensity shows a single exponential decay. Around the peak wavelength (478 to 488 nm) the intensity initially decays much faster and cannot be described by a single exponential decay.

These different decay rates lead to a red-shift of the spectrum during decay. Figure 5c shows three spectra from different time windows: during the pulse, shortly after the pulse is switched off, and close to the end of the streak camera image. Therefore these spectra correspond to different carrier densities. The red-shift and broadening of the spectra during the decay is evident. High resolution cw spectra of an identical 470 nm LD are shown in Fig. 6 for comparison. The thick black area results from thousands of longitudinal modes with a mode spacing of  $\approx 0.04$  nm, which are spectrally resolved in this measurement.<sup>19</sup> A spectrometer with lower resolution would average over the longitudinal modes. The close relation between the spectra taken with the streak camera (see Fig. 5c) and with the high resolution spectrometer (see Fig. 6) is obvious. Thus the origin of the narrowing and blue-shift is the increasing contribution of the amplified spontaneous emission. This also proves that the origin of the wavelength dependency of the decay rate is stimulated emission. The faster decay at shorter wavelengths reflects the increasing optical gain.

Of course, the waveguide of the LD confines light very well and therefore promotes stimulated emission. But stimulated emission will also play a role in LEDs with guided modes in the epitaxial plane<sup>2</sup> and at high carrier densities. For many experiments with pulsed optical excitation the carrier density can only be estimated, because absorption, excitation intensity, and spot size are not precisely known and because the system does not reach a stationary state. A wavelength dependency of the carrier lifetime frequently observed in those experiments is usually explained by carrier localization.<sup>20,21</sup> From our experiments we would argue that stimulated emission is the reason for the wavelength dependent carrier lifetime.

#### 4. SLOPE EFFICIENCY AND CARRIER INJECTION

The slope efficiency of the LD allows one to estimate the injection efficiency. Above threshold the optical power of a LD is given by

$$P_{opt} = \frac{h\nu}{q_e} \eta_d (I - I_{th}) = \frac{h\nu}{q_e} \frac{\alpha_m}{\alpha_m + \alpha_i} \eta_{inj} (I - I_{th}) \quad (6)$$

where  $\eta_d$  is the differential efficiency, and  $\alpha_m$  and  $\alpha_i$  are the mirror and internal losses, respectively. The slope efficiency of these 470 nm LDs is typically  $h\nu\eta_d/q_e = 0.45$  W/A, with minimal and maximal values of  $h\nu\eta_d/q_e = 0.2$  W/A and  $h\nu\eta_d/q_e = 0.8$  W/A, respectively.<sup>22</sup> The 470 nm LD has mirrors with relatively high reflectivity in order to reduce the threshold current density. Mirror losses are of the order of  $\alpha_m \approx 1.6$  cm<sup>-1</sup>. Internal losses  $\alpha_i \approx 20$  cm<sup>-1</sup> were measured with the Hakki-Paoli method.<sup>15,17</sup> These values result in

$$\frac{h\nu}{q_e} \eta_d = \frac{h\nu}{q_e} \frac{\alpha_m}{\alpha_m + \alpha_i} \eta_{inj} = \eta_{inj} 0.20 \text{ W/A} \quad (7)$$

The typical slope efficiency 0.45 W/A is higher than this value. Therefore mirror losses must be higher and/or internal losses lower than the values given above. A value of the injection efficiency considerably lower than 1 can be ruled out, as it would lead to values of the mirror reflectivity or internal losses which are in strong conflict with the measured values.

The question remains if this high injection efficiency in the lasing regime rules out injection losses as origin for the droop of a LED. If the carriers never reach the active region (“lack of hole injection”<sup>8</sup>) or if the length of stay of the overflowing carriers is negligible, the low injection efficiency should apply for the LD as well as for the LED. Yet, if the injection loss is caused by a (thermal) spill-over process, where the length of stay of the carriers in the QW is comparable to the carrier life time, than the argument with the slope efficiency is no longer valid. In that case there will be a competition between stimulated emission and scattering out of the quantum well. If stimulated emission is fast enough, carrier overflow can be suppressed, similar to the suppression of Auger losses by stimulated emission. In the competition between the different recombination or loss mechanisms, always the fastest process will win, which in the case of the LD above threshold is the stimulated emission.

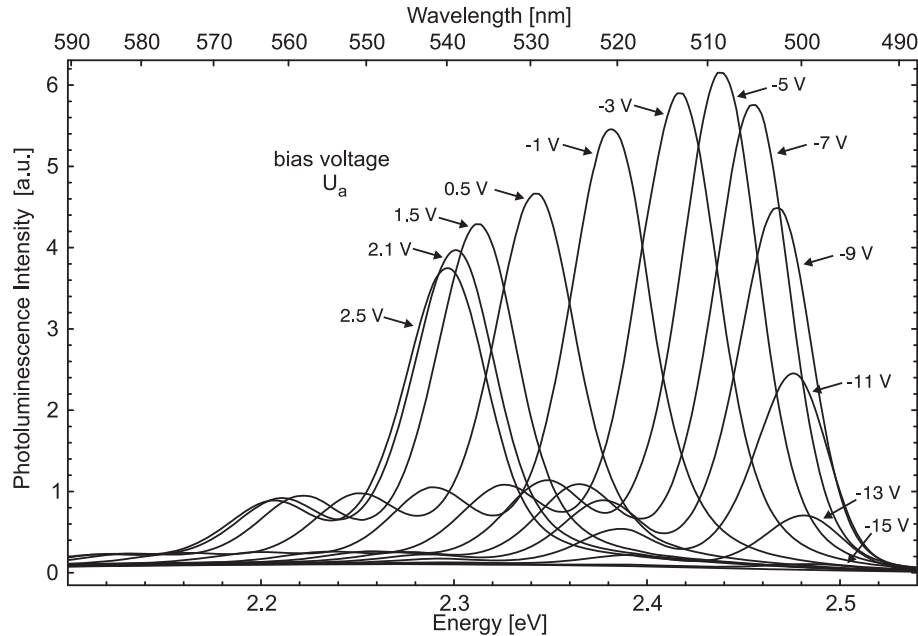


**Figure 7.** E-field dependent photoluminescence spectra. Bias voltage was varied from  $U_{bias} = -15$  V to  $U_{bias} = 2.5$  V. For selective excitation of the QWs the excitation wavelength was 380 nm. The measurements were carried out at low temperature,  $T = 8$  K. At  $U_{bias} = 2.5$  V electroluminescence begins to contribute to the signal.

## 5. INFLUENCE OF BUILT-IN POTENTIAL ON CARRIER DECAY

The field inside the active region and in particular inside the quantum wells is determined not only by the piezoelectric field but also by the field due to the built-in potential of the pn junction. Both are of the same order of magnitude. The built-in potential can be modulated by the bias voltage applied to the diode. The drastic effect of this is evident in photoluminescence spectra with applied bias, as shown in Fig. 7. There the photoluminescence is shown for a 540 nm green LED structure. The spectra were measured at low temperature ( $T = 8$  K) and show the characteristic phonon replica at the low energy side. Bias voltage was varied from  $U_{bias} = -15$  V reverse bias to the onset of electroluminescence at  $U_{bias} = 2.5$  V. The spectra show a blue shift of more than 40 nm with increasing bias voltage. The reason for this shift is the compensation of the piezoelectric field by the field of the pn junction. At  $U_{bias} = -15$  V the quantum well is nearly flat.

For bias voltage varying from  $U_{bias} = 2.5$  V forward bias to  $U_{bias} = -5$  V reverse bias, the photoluminescence signal is increasing with decreasing bias. The reason is the increasing radiative recombination rate due to a larger overlap of electron and hole wavefunctions. For more negative bias the photoluminescence intensity decreases fast because carriers are tunneling out of the quantum wells. This tunneling rapidly quenches the photoluminescence signal.<sup>23,24</sup>

As a consequence, one has to be careful when drawing conclusions from photoluminescence measurements for the electroluminescence of a LED. In electroluminescence the LED or LD is usually operated with dc or quasi dc forward bias. Photoluminescence can be measured with open contact, forward, or reverse bias. As Fig. 7 demonstrates, the photoluminescence spectra strongly depend on the variation of the field in the active region due to bias voltage.

An interesting mode is to measure electroluminescence with electric pulses with rise and fall times faster than the carrier life time. In that case transit electroluminescence can be measured with zero or negative bias. In

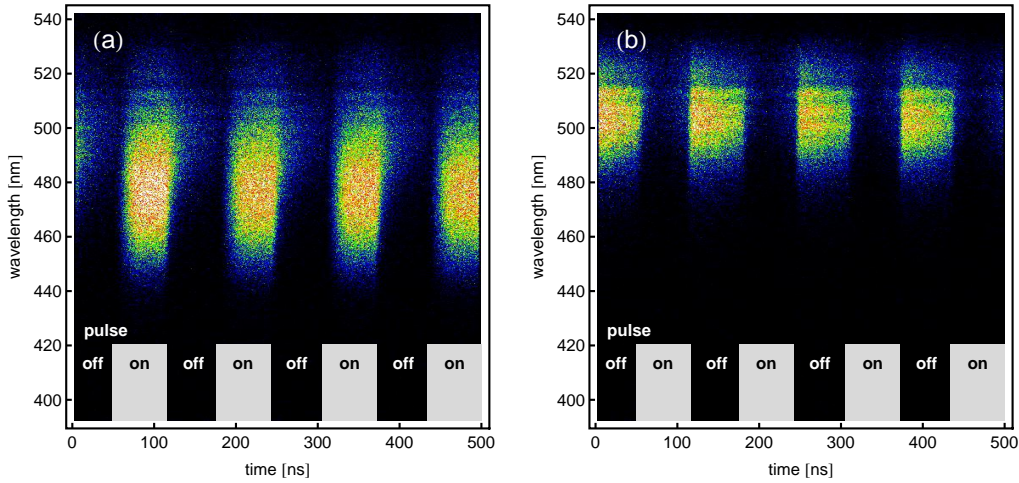


**Figure 8.** [Color online] Streak camera image of the LD470 driven with a 8 MHz rectangular driving pulse. (a) close to threshold, (b) far below threshold. The current densities are  $1.7 \text{ kAcm}^{-2}$  and  $0.14 \text{ kAcm}^{-2}$ , respectively. The gray bars along the time axis mark the ‘on’ and ‘off’ times.

the low to intermediate current regime, where the carrier lifetime is several 10 ns or 100 ns, this can be readily achieved with fast pulse generators.

One interesting consequence is that a LED driven with a pulse sequence may emit more light during the time when no current is flowing (zero bias) as compared to the time when current is flowing (forward bias).<sup>11</sup> The explanation of this effect is straightforward: during the driving pulse the quantum well is tilted, the wavefunction overlap is small, and the radiative recombination rate is low. After the pulse, at zero bias, the field of the pn junction reduces the field inside the quantum well, and the radiative recombination rate increases. We observed an increase of the intensity by a factor of 7 and more at the trailing edge of the driving pulse.<sup>11</sup>

This switching of the radiative recombination rate and wavelength during pulsed operation is most evident in streak camera traces as shown in Fig. 8. The axes are time and wavelength. Along the time axes the ‘on’ and ‘off’ times of the 8 MHz rectangular driving pulse are marked. Figure 8a shows the 470 nm LD at a current slightly below threshold. The electroluminescence signal is strongest during the pulse. The relative position of the electrical and optical pulse on the time axis are known from lasing operation (not shown in Fig. 8), where the usual relaxation oscillations are an unambiguous signal for a normal onset of lasing during the driving pulse.

For the low driving current in Fig. 8b, bright and dark phases are shifted by  $\pi$ , i.e. the emission takes place at zero bias while the LD is dark during forward bias. With a 1 GHz oscilloscope we checked that the electrical pulse remains rectangular and is neither shifted nor distorted.

From the comparison of Fig. 8a and b the blue shift of the emission for currents close to  $I_{th}$  is obvious. The LD emitting at 470 nm close to the peak of the emission in Fig. 8a becomes a green LED for low current densities (see Fig. 8b). Also the red shift at the end of each pulse is clearly visible in Fig. 8a. This is identical to the behavior shown in Fig. 5.

Spectrally integrated time trace and spectral position as function of time are shown in Fig. 9a and b, respectively. The spectral position was calculated by taking the first momentum of the spectra.<sup>25</sup> For high current density the intensity rises and falls fast. This is similar to the time trace of the green LED in Fig. 4. However, both rise and fall time are shorter, the rise time because of the higher current density, the fall time because of stimulated emission.

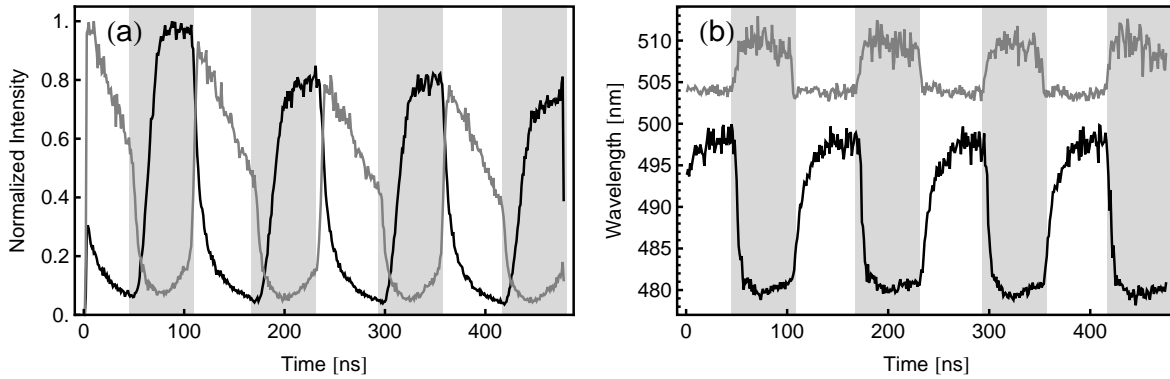


**Figure 9.** (a) intensity and (b) energy of electroluminescence as function of time. The traces are taken from the streak camera measurement shown in Fig. 8. The ‘on’ time of the driving pulse is marked by gray areas.

The low current time trace in Fig. 9 is dramatically different. Please be aware that the intensity of both traces are normalized. The absolute intensity of the low current trace is much lower. The intensity rises slowly during the driving pulse, due to the low driving current and consequently long carrier life time (see Fig. 3). At the end of the 125 ns long pulse the system is still not in equilibrium. After the trailing edge the intensity rises almost instantaneously. This is caused by a change of the recombination rate due to the switching of the field in the quantum wells. The switching time is much shorter than the decay time after the pulse. Therefore the change of the carrier density during switching can be neglected. This way one can measure the decay time with a given carrier density as function of bias voltage.<sup>11</sup> During off time of the driving pulse the carrier density and consequently intensity decays with the rate given by the configuration of the quantum well with zero bias. At the leading edge of the following pulse the quantum well is switched back to the forward bias configuration, and the intensity drops fast due to the change in the recombination rates.

This switching of the quantum well configuration can also be seen in the trace of the center wavelength, Fig. 9b. For the low current trace, the emission during forward bias is red shifted, compared to zero bias due to the QCSE. For forward bias the field due to the built-in potential is low and the QW experiences a strong tilt due to the piezoelectric polarization (QCSE). For zero bias this field is partially compensated, resulting in a smaller tilt of the QW. The wavelength shift for high current is opposite, reflecting the shape of the optical gain curve which is determined by the density of states, homogeneous and inhomogeneous broadening.<sup>12, 13, 15</sup>

The intensity rise at the trailing edge of the pulse is not a particular feature of the LD, but exists as well in a LED.<sup>11</sup> The lowest two traces in Fig. 4 show an increased intensity after the pulse (this is better visible on a linear scale) which becomes more pronounced at lower current densities. The fact that this increase of the radiative recombination rate after the pulse is already suppressed at moderate current densities indicates that the internal field is already largely screened.

The fast decay after the pulse for zero bias cannot be due to tunneling, because then the intensity would drop at the trailing edge. When switching from forward to reverse bias an onset of tunneling can be observed. Then the decay time becomes very fast, and the peak intensity after the pulse does not increase anymore.

The time trace of the electroluminescence intensity at a slightly higher current density than in Fig. 8b is shown in Fig. 10 together with a simulation of the time dependent radiative current. The electroluminescence intensity is again rising and falling nearly instantaneously at the trailing and leading edge of the driving pulse, respectively. The simulated time trace is curve is a solution of the rate equation 1. The parameters are the ones for LD470 from table 1 with the exception of the radiative recombination rate. During the ‘on’ times (forward bias) of the driving pulse we used the same rate  $B = 2 \times 10^{-7} \text{ cm}^2 \text{ ns}^{-1}$  as above. During ‘off’ times (zero bias) this radiative recombination time was tripled,  $B = 6 \times 10^{-7} \text{ cm}^2 \text{ ns}^{-1}$ . The simulation reflects roughly the basic

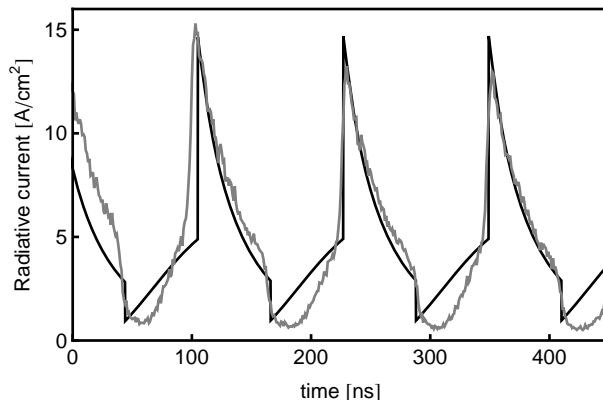


**Figure 10.** Measured electroluminescence intensity for LD470 (black) and simulated time trace of the radiative current (gray). The LD470 is driven with a 8 MHz square wave signal at a current density of  $0.35 \text{ kAcm}^{-2}$ . For the simulation the radiative recombination rate was tripled during the ‘off’ times (zero bias) of the driving current.

features of the experiment: the switching of the radiative current at the edges of the driving pulse and the faster decay during the ‘off’ times. A true simulation of the trace during the pulse would also need to include the simulation of the equivalent circuit of the LED and driving unit.

## 6. DISCUSSION & CONCLUSIONS

We demonstrated that electroluminescence measurements can be an important experiment to reveal recombination mechanisms and shed light on efficiency and losses. Time-resolved electroluminescence measurements have several advantages over time-resolved photoluminescence spectroscopy: current density can be precisely measured; the system can reach equilibrium (steady state) before measuring decay. Streak camera measurements also provide the spectral information in addition to the temporal one.

We measure lifetime for LEDs and LDs from very low carrier density, where Shockley–Read–Hall recombination dominates, to laser threshold. A increase of the recombination rate was observed, as expected in the standard rate equation model. We also observe the influence of stimulated emission on the shape of the spectra and on carrier life time already considerably below threshold carrier density. By comparison with Hakki–Paoli spectroscopy we demonstrated that the wavelength dependent lifetime observed across the spectrum is caused by stimulated emission.

As consequence of the QCSE, bias voltage affects the recombination rates. A strong ( $3\times$ ) modulation of the radiative recombination rate was observed for a green LED driven with a 8 MHz square wave. This modulation of the radiative recombination rate leads under certain conditions to the seemingly bizarre situation that the LED emits more light in the ‘off’ state (zero bias) than in the ‘on’ state (forward bias).

Stimulated emission and bias dependent recombination rates have to be considered when interpreting pulsed photoluminescence experiments. The wavelength dependent life time frequently observed in ultrashort pulse experiments might be due to stimulated emission, as demonstrated by our electroluminescence experiments.

Efficiency and color rendering index (CRI) of LEDs could possibly be improved by a modulated driving scheme. For the current LED design with narrow QWs we did not observe an absolute increase in efficiency upon modulated operation. Yet for LEDs with wider QWs, modulated operation might be one way to combine low carrier densities with high radiative recombination rates. The spectral shift during modulated operation would then also spectrally broaden the emission, such improving the CRI.

The presented lifetime data as function of current density is not accurate enough to determine the transition from radiative emission  $\propto BN^2$  to Auger-like losses  $\propto CN^3$ . For the measured LED the high current density regime was not accessible. For the LD the transition to stimulated emission sets in where the deviation from the  $\propto BN^2$  law becomes significant. This poses the question if stimulated emission could be the culprit for the fast recombination in the high carrier density regime. The LD could certainly be described without the  $\propto CN^3$  term if stimulated emission is taken into account in the rate equation. For the LEDs the fast recombination is necessary to describe the droop. Stimulated emission in a LED is fast and would be preferably in the epitaxial plane. In-plane light suffers from low extraction efficiency and high absorption. With this mechanism a redistribution of photons by stimulated emission could be a source of additional losses at high current densities. One consequence would be a narrowing of the edge emission which could be readily verified in an experiment. The considerable variation in the  $C$  parameter from sample to sample is a hint that the loss mechanism is not a material property but depends on the structure.

In terms of lifetime, carrier density, and spectra we see a smooth transition from LED to LD operation. Our measurements show that an Auger-like recombination term is not in conflict with laser operation. From slow efficiency of the LD follows a injection efficiency close to  $\eta_{inj} = 1$  for laser operation. Yet, this is not in immediate conflict with injection as possible source of droop in LEDs, as stimulated emission in LDs can also quench carrier overflow.

The spectrally resolved lifetime measurements are only one part of the puzzle to “uncover[ing] the LED’s darkest side.”<sup>26</sup> Yet they offer plenty of detailed information. Streak camera measurements as function of bias voltage and temperature, as well as for semipolar and nonpolar QWs could provide even more cues towards an understanding of the mechanisms responsible for the drop of the efficiency of InGaN QWs in the high current density and green spectral region, the so called “green gap”.<sup>27</sup>

## ACKNOWLEDGMENTS

First, I thank K. Kojima. The measurements of this article are part of our measurement campaign in summer 2007. While we published other aspects of our work, we never got around to evaluate the life time measurements. Harald Braun contributed the E-field dependent spectra — thank you very much. I acknowledge stimulating discussions with M. Sabathil, in particular his suggestion to include slope efficiency. The author acknowledges support through an invited fellowship from the Japan Society for the Promotion of Science (JSPS). This work was in part supported by the Deutsche Forschungsgemeinschaft (DFG) within the research group POLARCON.

## REFERENCES

1. J. M. Phillips, M. E. Coltrin, M. H. Crawford, A. J. Fischer, M. R. Krames, R. Mueller-Mach, G. O. Mueller, Y. Ohno, L. E. S. Rohwer, J. A. Simmons, and J. Y. Tsao, *Research challenges to ultra-efficient inorganic solid-state lighting*, Laser & Photonics Reviews **1**, 307 (2007).
2. Ch. Wiesmann, K. Bergeneck, N. Linder, and U. T. Schwarz, *Photonic crystal LEDs - designing light extraction*, Laser & Photonics Reviews (2009), doi:10.1002/lpor.200810053.
3. N. F. Gardner, G. O. Müller, Y. C. Shen, G. Chen, S. Watanabe, W. Götz, and M. R. Krames, *Blue-emitting InGaNGaN double-heterostructure light-emitting diodes reaching maximum quantum efficiency above 200 A/cm<sup>2</sup>*, Appl. Phys. Lett. **91**, 243506 (2007).
4. J. Hader, J. V. Moloney, B. Pasenow, S. W. Koch, M. Sabathil, N. Linder, and S. Lutgen, *On the importance of radiative and Auger losses in GaN-based quantum wells*, Appl. Phys. Lett. **92**, 261103 (2008).
5. M.-H. Kim, M. F. Schubert, Q. Dai, K. Kim, E. F. Schubert, J. Piprek, and Y. Park, *Origin of efficiency droop in GaN-based light-emitting diodes*, Appl. Phys. Lett. **91**, 183507 (2007).
6. M. F. Schubert, S. Chhajed, J. K. Kim, E. F. Schubert, D. D. Koleske, M. H. Crawford, S. R. Lee, A. J. Fischer, G. Thaler, and M. A. Banas, *Effect of dislocation density on efficiency droop in GaInN/GaN light-emitting diodes*, Appl. Phys. Lett. **91**, 231114 (2007).
7. L. Wang, J. Wang, H. Li, G. Xi, Y. Jiang, W. Zhano, Y. Han, and Y. Luo, *Study on Injection Efficiency in InGaN/GaN Multiple Quantum Wells Blue Light Emitting Diodes*, Appl. Phys. Express **1**, 021101 (2008).

8. J. Xu, M. F. Schubert, A. N. Noemaun, D. Zhu, J. K. Kim, E. F. Schubert, M. H. Kim, H. J. Chung, S. Yoon, C. Sone, and Y. Park, *Reduction in efficiency droop, forward voltage, ideality factor, and wavelength shift in polarization-matched GaInN/GaInN multi-quantum-well light-emitting diodes*, Appl. Phys. Lett. **94**, 011113 (2009).
9. S.-I. Nagahama, T. Yanamoto, M. Sano, and T. Mukai, *Wavelength dependence of InGaN laser diode characteristics*, Jpn. J. Appl. Phys. **40**, 3075 (2001).
10. S.-I. Nagahama, Y. Sugimoto, T. Kozaki and T. Mukai. *Recent progress of AlInGaN laser diodes*, Proc. SPIE **5738**, 57 (2005).
11. U. T. Schwarz, H. Braun, K. Kojima, Y. Kawakami, S. Nagahama, and T. Mukai, *Interplay of built-in potential and piezoelectric field on carrier recombination in green light emitting InGaN quantum wells*, Appl. Phys. Lett. **91**, 123503 (2007).
12. B. Witzigmann, M. Tomamichel, S. Steiger, R. G. Veprek, K. Kojima, and U. T. Schwarz, *Analysis of gain and luminescence in violet and blue GaInN/GaN quantum-wells*, IEEE J. Quantum Electronics **44**, 144 (2008).
13. J. Hader, J. V. Moloney, and S. W. Koch, *Influence of internal fields on gain and spontaneous emission in InGaN quantum wells*, Appl. Phys. Lett. **89**, 171120 (2006).
14. J. V. Moloney, J. Hader, and S.W. Koch, *Quantum design of semiconductor active materials: laser and amplifier applications*, Laser & Photonics Reviews **1**, 4 (2007).
15. K. Kojima, U. T. Schwarz, M. Funato, Y. Kawakami, S. Nagahama, T. Mukai, *Optical gain spectra for near UV to aquamarine (Al,In)GaN laser diodes*, Optics Express **15**, 7730 (2007).
16. K. Kojima, M. Funato, Y. Kawakami, S. Nagahama, T. Kumai, H. Braun, U. T. Schwarz, *Gain suppression phenoma observed in InGaN QW laser diodes emitting at 470 nm*, Appl. Phys. Lett. **89**, 241127 (2006).
17. U. T. Schwarz, H. Braun, K. Kojima, M. Funato, Y. Kawakami, S. Nagahama, T. Mukai, *Investigation and comparison of optical gain spectra of (Al,In)GaN laser diodes emitting in the 375 nm to 470 nm spectral range*, Proc. SPIE **6485**, 648506 (2007).
18. U. T. Schwarz, E. Sturm, W. Wegscheider, V. Kümmler, A. Lell, and V. Härle, *Excitonic signature in gain and carrier induced change of refractive index spectra of (In,Al)GaN quantum well lasers*, Appl. Phys. Lett. **85**, 1475 (2004).
19. U. T. Schwarz, E. Sturm, W. Wegscheider, V. Kümmler, A. Lell, and V. Härle, *Gain spectra and current-induced change of refractive index in (In/Al)GaN diode lasers*, phys. stat. sol. (a) **200**, 143 (2003).
20. Y. Kawakami, K. Omae, A. Kaneta, K. Okamoto, Y. Narukawa, T. Mukai, and S. Fujita, *In inhomogeneity and emission characteristics of InGaN*, J. Phys.: Condens. Matter **13**, 6993 (2001).
21. T. Hino, T. Asano, T. Tojyo, S. Kijima, S. Tomiya, T. Miyajima, S. Uchida, and M. Ikeda, *Estimation of Device Properties in AlGaInN-Based Laser Diodes by Time-Resolved Photoluminescence*, phys. stat. sol. (a) **188**, 101 (2001).
22. Nichia Inc., product guide for aquamarine laser diode NDHA210APAE1.
23. A. Laubsch, M. Sabathil, G. Bruederl, J. Wagner, M. Strassburg, E. Baur, H. Braun, U. T. Schwarz, A. Lell, S. Lutgen, N. Linder, R. Oberschmid, and B. Hahn, *Measurement of the internal quantum efficiency of InGaN quantum wells*, Proc. SPIE **6486**, 64860J (2007).
24. M. Sabathil, A. Laubsch, and N.Linder, *Self-consistent modeling of resonant PL in InGaN SQW LEDstructure*, Proc. SPIE **6486**, 64860V (2007).
25. N. Gmeinwieser, K. Engl, P. Gottfriedsen, U. T. Schwarz, J. Zweck, W. Wegscheider, S. Miller, H.-J. Lugauer, A. Leber, A. Lell, and V. Härle, *Correlation of strain, wing tilt, dislocation density, and photoluminescence in epitaxial lateral overgrown GaN on SiC substrates*, J. Appl. Phys. **96**, 3666 (2004).
26. M. Schubert, M.-H. Kim, J. K. Kim, and E. F. Schubert, *Uncovering the LED's darkest secrets*, Compound semiconductors **Vol. 13**, No. 11, p. 19 (2008).
27. M. Peter, *Osram explores the route to high-performance greens*, Compound semiconductors **Vo. 13**, No. 6, p. 16 (2008).